Polymer Vol. 30 No. 13, pp. 2733–2744, 1998
© 1998 Elsevier Science Ltd
Printed in Great Britain. All rights reserved
0032-3861/98/$19.00+0.00
PII: S0032-3861(97)00613-7

Layer by layer imaging of diblock copolymer films with a scanning electron microscope

Christopher Harrison[a,*], Miri Park[a], P. M. Chaikin[a], Richard A. Register[b], Douglas H. Adamson[c] and Nan Yao[c]
[a]Department of Physics, Princeton University, Princeton, NJ 08544, USA
[b]Department of Chemical Engineering, Princeton University, Princeton, NJ 08544, USA
[c]Princeton Materials Institute, Princeton University, Princeton, NJ 08544, USA
(Received 7 November 1996; revised 17 July 1997)

We present a novel technique which allows for the investigation of block copolymer microstructures on various substrates and at different depths. Using a low voltage, high resolution scanning electron microscope (SEM), we examined the topography and underlying morphology of poly(styrene)–poly(butadiene) diblock copolymer films. The internal morphology of the film was exposed for SEM imaging by using a non-selective fluorine-based reactive ion etching (RIE) technique. By controlling the depth of the RIE etch we removed the surface layer of poly(butadiene) and exposed the microphase separated structure underneath for SEM imaging. After obtaining SEM images of this exposed layer, we subsequently removed this layer with further RIE to obtain SEM images of the layer underneath. By continuing this procedure, we can obtain images of the microstructures as a function of depth with a 4-nm lateral resolution and a 10-nm depth resolution. © 1998 Elsevier Science Ltd. All rights reserved.

(Keywords: diblock copolymer films; scanning electron microscope; reactive ion etching)

INTRODUCTION

Diblock copolymer systems with a narrow polydispersity ($M_w/M_n \sim < 1.1$) and with $\chi N > 10$ microphase separate above their glass transition temperature, where χ is the Flory–Huggins interaction parameter and N is the degree of polymerisation[1]. The resulting morphology depends largely on the relative volume fractions of the components. Some of the more commonly seen morphologies are lamellae, cylinders and spheres. These morphologies have been studied in bulk samples by a variety of techniques, but only within the past decade have the morphologies of these polymers been examined in thin films on substrates, where new effects have been observed[2]. For example, there has been a recent interest in surface-induced ordering of diblock copolymer films[3] and the effect of the free surface on the microphase morphology of thin films[4]. In addition, a dependence of the morphology on the film thickness has been observed by our group[5] and others[6]. In these studies, it has been difficult to directly image the multiple layers of microstructures with conventional transmission electron microscopy (TEM) techniques. Recently, tomography has been employed in order to obtain images of layered microstructures, but this technique is unsuitable for examining thin films on substrates[7]. Thin film structures have also become increasingly interesting for lithographic processes which pattern substrates at a length-scale previously inaccessible to researchers[8]. Therefore, a technique which can directly image each layer of microstructures independently while on a substrate would further our understanding of thin films and assist in block copolymer lithography.

The study of block copolymers has employed many techniques, ranging from X-ray scattering, neutron reflectivity, atomic force microscopy, and TEM[1]. The imaging of block copolymer microstructures with feature sizes of 10–60 nm has traditionally been accomplished by TEM, which has proven to be an excellent tool for studying these systems due to its high resolution (≈0.15 nm). Though TEM provides a high resolution image, the investigator quickly runs into certain limitations. Because a TEM requires that the electrons pass through the sample, the investigator is limited to a thin specimen (less than 1 micron), typically prepared by placing it onto a carbon-coated TEM grid, or more recently, directly spin coated on a silicon nitride window[9]. Therefore a TEM cannot easily image the morphology of polymer films on a comparatively thick substrate such as a silicon wafer. In addition, conventional TEM has difficulty obtaining a separate image of each layer of microstructures. Though for some substrates, the polymer films can be floated off and microtomed for such analysis, the minimum thickness of microtomed sections appears to be about 70 nm, several times the typical periodicity of microstructures. TEM images consisting of projections of thin films which contain overlapping layers of microstructures are often difficult to interpret. In contrast, with the technique presented in this paper, an individual image of each layer can easily be obtained without removal of the entire film from the substrate.

The scanning electron microscope (SEM), an ideal tool for imaging microscopic surface features, has not been as extensively used in the study of polymer microstructures. Though the lateral resolution of a SEM is lower, it overcomes certain inherent limitations of the TEM. The SEM can image polymer films over a wide range of thicknesses on any substrate since it is a surface imaging tool and the information is coming from electrons escaping the sample surface, not from the transmitted electrons as

* To whom correspondence should be addressed

with TEM. Until recently, the SEM could not operate with the necessary combination of low voltage (1–5 kV) and high resolution (~4 nm) needed to effectively image non-conducting polymer systems with a typical feature size of 10 nm. The imaging of non-conducting polymer systems is done at low voltage in order to minimise charging effects which can obscure the image. The recent development of the field emission gun SEM and the corresponding increase in its resolution at low voltage has launched new techniques by which polymer systems can be examined. The excitement of the polymer community about the use of low voltage, high resolution SEM is evident in the number of recent publications concerning SEM polymer imaging techniques[10–13].

Efforts other than our own have been made to image block copolymer microstructures with an SEM. Lai *et al.* showed that an SEM can be used to image poly(styrene)–poly(butadiene) block copolymer systems, but this work was restricted to imaging microstructures that were within the top ~30 nm of the surface[14]. Thomas *et al.* showed that an SEM can obtain images of a poly(styrene)–poly(butadiene) symmetric block copolymer system if the lamellae were oriented perpendicular to the film[10], but again, only surface images were obtained. In this work, the contrast was produced by the topography of the corrugations of the perpendicular lamellae and enhanced by OsO_4 staining of the poly(butadiene) domains. We find that the SEM (without etching the polymer film) can effectively image the internal microstructures only within the top 30 nm of the surface, preventing one from imaging the individual layers of microstructures independently in a film which contains multiple layers of microstructures. Therefore, we were motivated to develop a new imaging technique which allows us to examine layers of diblock copolymer microstructures in thin films on substrates.

In this paper we present studies of three diblock copolymers in thin films which we imaged using a technique that combines a reactive ion etcher (RIE) and SEM (the RIE/SEM technique). In order to investigate the internal morphology of a diblock copolymer film, an etching technique is used which exposes the microdomains to the surface for SEM imaging. By alternating between SEM imaging and RIE polymer removal, we can obtain layer by layer images as a function of depth.

SAMPLE PREPARATION

Three diblock copolymers were synthesised by standard high-vacuum anionic techniques in a cyclohexane/benzene ($90/10^{v}/_{v}$) mixture to yield a high 1,4 content in the polydiene blocks[15]. The first diblock copolymer (SB 36/11) was synthesised with a composition of 36 kg/mol for the poly(styrene) (PS) block and 11 kg/mol for the poly(butadiene) (PB) block such that microphase separation produces PB cylinders in a matrix of PS. The second PS–PB diblock copolymer (SB 65/10) was synthesised with a composition of approximately 65 kg/mol for the PS block and 10 kg/mol for the PB block. This diblock copolymer microphase separates to produce a morphology consisting of PB spheres in a PS matrix. The third diblock copolymer (SI 68/12) was synthesised with a composition of 68 kg/mol for the PS block and 12 kg/mol for the poly(isoprene) (PI) block such that microphase separation produces PI spheres in a PS matrix. The diblock copolymers were dissolved in toluene, a good solvent for the polymer blocks. For SEM work, we prepared thin polymer films by spin coating polymer solutions on silicon substrates (previously cleaned with toluene) and subsequently annealing in a vacuum oven at 125°C for 24 h. Annealing at this temperature, which is above the glass transition temperature (100°C) of our polymers but below the order–disorder temperature, produces well-ordered microdomain structures. We controlled the film thickness by varying the solution concentration and spin speed of the spin coater (Headway Research International, model no. CB-15). Typical film thicknesses in our study ranged from 30 to 250 nm. After annealing our samples, we selectively stained the PB or PI component for 2 h with vapours of an aqueous 4% osmium tetraoxide solution (Polysciences). The osmium tetraoxide selectively stains the carbon–carbon double bonds in PB or PI domains and does not react significantly with the PS domains. Film thicknesses were measured by an ellipsometer (Gaertner, model no. L116C) or an interferometer (Leica, MPV-SP). Since the periodicity of the domains (~30 nm) was less than one-tenth of the wavelength of light used by the ellipsometer (~633 nm), the index of refraction measured by the ellipsometer was a volume average of the indices of refraction of the PB microdomains and the PS matrix. When using an interferometer, the user must specify the index of refraction, which we took from the value measured by the ellipsometer. Stained samples typically had an index of refraction of approximately 1.6, which is a volume average of the indices of refraction of the unstained PS matrix and the stained PB or PI domains.

For some of our depth profiling studies, silicon wafers were first coated with a 130-nm layer of poly(methyl methacrylate), PMMA. This layer was applied by spin coating a solution of 4% PMMA in anisole (Microlithography Chemical Corporation, M_w = 495 kg/mol) and subsequent vacuum annealing at 170°C for 4 h to remove the solvent. Next, a solution of SB 36/11 dissolved in toluene was spin coated on the PMMA coated substrate and annealed as mentioned previously to create a 240-nm thick block copolymer layer. Due to the rapidity of the spin coating process (~1 s), the toluene in the SB 36/11 solution did not significantly remove the PMMA, as measured by interferometry.*

Polymer film etching was performed at the Cornell Nanofabrication Facility (CNF) using a reactive ion etcher by Applied Materials. For the Applied Materials RIE, the etching process was performed at a CF_4 flow rate of 10 standard cubic centimeters per minute (SCCM), a pressure of 2 mtorr, and a power density of ≈ 0.03 watts/cm^2.† A self-bias of approximately 290 V developed between the anode and the cathode, on which the sample was placed. Typically, oxygen plasma etching is used for rapid etching of carbon based polymer films, but we chose CF_4 RIE with the above parameters in order to obtain a non-selective and smooth etching process and to achieve a sufficiently slow etching rate that allowed us to adequately control the etch depth.

*The PS–PB/PMMA bilayers were prepared and investigated for their applicability to pattern transfer. See, for example, Refs 5 and 8.

† In some cases we used a Plasma Therm System VII 790 series at the Advanced Technology Center for Photonics and Optoelectronic Materials (ATC/POEM) at Princeton University. For the Plasma Therm RIE, similar etching rates were obtained with a mixture of 90% CF_4 and 10% O_2 (this was the only available CF_4 mixture). RIE parameters in this case were 0.03 W/cm^2, 25 mtorr, 20 SCCM. The etching rate was 20 nm/min. For these parameters, stained PB and PS etch at slightly different rates and the etching process introduces non-negligible roughness to the polymer film. However, for the purposes of imaging the top layer of microstructures, these parameters suffice.

To calibrate the relative etching rates of the PB, PI and the PS blocks with CF_4 RIE, the etching rates of three homopolymers were studied, PS (synthesised by standard anionic techniques in benzene, M_w=161 kg/mol, polydispersity=1.05), PB (Scientific Polymer Products, $M_w \approx$ 420 kg/mol; 36% *cis*, 55% *trans*, 9% vinyl), and PI (synthesised by standard anionic techniques in cyclohexane, M_w = 85 kg/mol, polydispersity = 1.05). Homopolymer films were prepared in a similar way as the copolymer films, including annealing and staining. The etching rate was calibrated by measuring the thickness of the polymer film by an ellipsometer or interferometer before and after each 1-min interval of etching. We find that under the RIE conditions used for this work (see above) this dry etching process removes approximately 12 nm of the polymer film per minute for each of the unstained homopolymers. Though staining does not affect the etch rate of PS or PB, the stained PI block etches at a rate of 20 nm per minute under the given RIE conditions. This difference in the etching rates of PS and PI would prevent effective depth profiling in a stained PS–PI copolymer system, but it does not prevent one from etching away the PI surface wetting layer to effectively image the topmost layer of internal microstructures.

We also investigated O_2 RIE, a more typical means of etching away polymer films. In order to compare the effects of CF_4 RIE to O_2 RIE on the polymer microstructures, it was necessary to use a film without heavy metal staining agents that could affect the O_2 RIE etching rate. We prepared films of SB 36/11 as described previously, but instead of staining, we removed the PB cylinders with ozone[16], leaving voids in the PS matrix. This ozonation process does not roughen the film as observed by SEM and the higher resolution of a TEM. These ozonated films have shown great utility in nanolithography[8]. Next, we exposed the voids to the surface by etching with O_2 RIE or CF_4 RIE, allowing us to compare the effects of both etching processes. We attempted to set the etching conditions of O_2 RIE, such as power level and pressure, to be similar to our etching parameters for CF_4 RIE. The RIE parameters used were 10 mtorr, 0.03 W/cm^2, 30 SCCM of O_2, with a measured etching rate of approximately 50 nm/min for PS (previously treated with ozone, which increases its etching rate ~30% compared to untreated PS). As will be discussed in a following section, we found that O_2 RIE introduced significant roughness compared to CF_4 RIE.

The SEM images in this paper were obtained with a Leo Gemini 982 Field Emission Gun SEM at both CNF and the Centre for Ceramics Research at Rutgers University. The reported resolution at 1 KV is 4 nm. SEM work was performed with an incident electron beam energy between 1 and 5 kV and by collecting secondary electrons (SE) or when available, secondary plus back-scattered electrons (BSE). At higher operating voltages, the SE and BSE signal can be dramatically different, but at 1–5 kV, we could discern little difference in resolution between the two signals. A higher resolution was typically seen with the combined signals opposed to each signal independently because of the increased signal-to-noise ratio. Hence all further discussion, except in the section discussing the contrast mechanism, will refer only to the SE signal. The working distance was varied to optimise the contrast of the sample.

For dynamic Secondary Ion Mass Spectrometry (SIMS) analysis, SB 36/11 films were prepared as described previously. The samples were stained, and then a 23-nm thick sacrificial overlayer of deuterated PS (Cambridge Isotope Laboratories, M_w = 116 kg/mol, polydispersity = 4.7) was applied to allow the SIMS beam to warm up to full beam intensity before sputtering through to the SB 36/11 film. Analysis was done by Evans East with a Physical Electronics Phi-6300 using a 2-kV positively charged cesium beam at an angle of 60° from the sample surface normal in order to maximise the depth resolution. Negatively charged secondary ions were collected at a normal angle from the sample surface while sputtering the copolymer film at approximately 6 nm/min. In addition, a compensating electron beam was used to minimise charging at the sample surface. The total sputtered depth was determined with a profilometer. Assuming the carbon yield to be constant, all signals were normalised with the variation of the carbon yield from its average. The lateral dimensions of the region examined by SIMS were 500 by 500 μm.

SEM IMAGING OF THE TOP LAYER OF MICROSTRUCTURES

This section describes the use of the RIE/SEM technique to obtain images of block copolymer microdomains. For demonstration of this technique, a uniform SB 36/11 film consisting of two monolayers of cylindrical PB microstructures (with accompanying free and confined surface PB wetting layers, to be discussed further in a following section) was spun coat with an average thickness of 70 nm, annealed, and stained. This sample, when imaged by an SEM using secondary electrons at 1 kV, shows little surface contrast, for the polymer film is both chemically uniform at its surface and topographically flat (*Figure 1a*).‡ This uniformity in signal is indicated by the arrows in the cross-sectional schematic of *Figure 1a*. In the middle of *Figure 1a* there is a 40-nm gold sphere applied to the polymer surface from a colloidal solution to aid in SEM beam alignment. We use this sphere as an indicator that we are focusing the SEM at the surface of the polymer film with sufficient resolution to detect surface topography and microstructures. The microstructures underneath the wetting layer do not produce measurable surface corrugations in this system.

In an SEM, incident electrons interact with the sample and produce SEs which are collected by a detector. Contrast is produced by the higher electron yield from the stained PB cylinders as compared to the lower yield of the PS matrix. At an incident beam energy of 1 keV, the electron range, or in this case the sampling depth (because of the low incident beam energy), is typically less than 15 nm[12], so few incident electrons will reach the PB cylinders submerged in the polymer film to produce a signal. In addition, electrons produced in the submerged stained PB cylinders will be less likely to emerge to the surface and be collected by the SEM detector. Lastly, the surface layer of stained PB, the lower surface tension block, produces a large SE signal, further hindering detection of any spatial contrast in SE signal produced in the submerged cylinders underneath.

To image the cylinders beneath the surface, we remove

‡ Spin coating a film at a thickness greater or less than needed for integer numbers of layers of cylinders can produce 'islands' and 'holes', respectively, during the annealing process. The typical lateral size of islands and holes that form due to this diblock copolymer (SB 36/11) film's quantised thickness is on the order of microns, after annealing for 24 h. These islands and holes can be imaged by the SEM, but this surface topography is at a lateral length scale that is more than an order of magnitude larger than the microstructures.

this surface layer by subjecting the film to a CF_4 reactive ion etcher (RIE) (*Figure 2*) which then exposes the underlying microdomains. An RIE[17] combines both the physical sputtering of an ion mill and the chemically reactive nature of plasma to remove the surface layer of the polymer film. The operating parameters of the RIE are described in the 'Sample preparation' section. In *Figure 1b*, we have removed 7 nm of the polymer film and the contrast due to

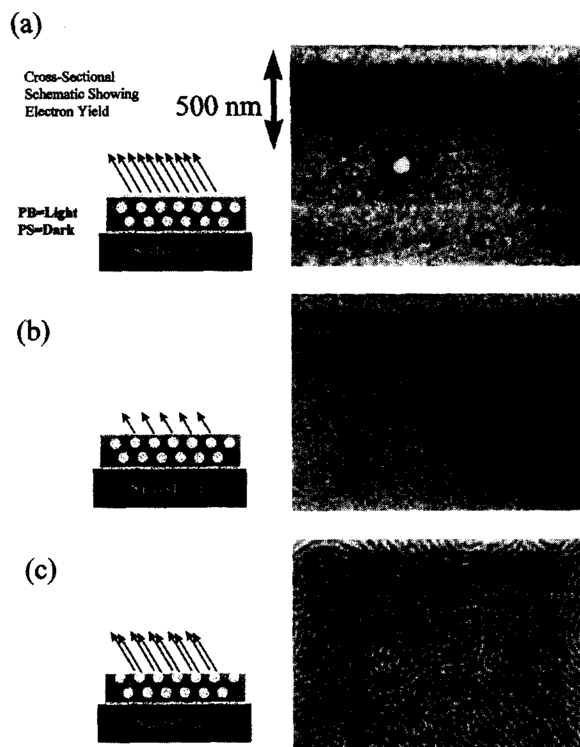

Figure 1 (a) A cross-sectional schematic of the SEM examining a polymer film two cylinder layers thick with an accompanying SEM image. Without etching away the PB surface layer, there is no microstructure contrast, as indicated with the uniform arrows in the schematic. A gold sphere that can be seen in the middle of the image establishes that we are imaging the polymer surface with sufficient resolution. (b) After etching 7 nm away, the microstructures can be discerned, but with poor contrast. (c) After 12 nm of etching, the cylinders have been exposed to the surface, optimizing the contrast. The arrows in the schematic correlate with the electron yield from the stained PB cylinders which appear light in the SEM image. (SEM voltage: 1 kV)

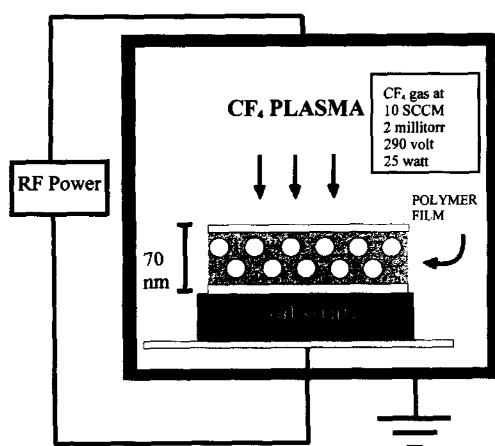

Figure 2 Schematic of a reactive ion etcher. The etch rate of the polymer film is 12 nm/min, which removes approximately one layer of cylinders for every two minutes of etching.

the stained cylinders has begun to emerge, represented in the schematic by the short arrows which correspond to a small modulation in intensity due to the cylindrical microstructures which are still not completely exposed to the surface. The images of *Figure 1a–c* do not correspond to the same location on the polymer film, but the same level of contrast in the SEM images of the microstructures was seen after each etching step regardless of the sample location.

Finally, after etching away 12 nm of the polymer film, the surface layer of PB and part of the PS matrix is removed, exposing the underlying cylinders to the surface for optimal contrast. A schematic of the film's surface, after etching, is shown in *Figure 1c* with accompanying double long arrows which represent the increased SE intensity of the exposed stained PB cylindrical microstructures. The stained PB cylinders (appearing light in SEM image) have a higher SE yield than the PS (appearing dark) due to the presence of osmium (atomic number 76). The contrast is produced by the spatial variation in average atomic number, which will be further discussed in the 'Contrast mechanism' section. Without staining, PB and PS are atomically quite similar and produce similar SE yields. In *Figure 1*, the cylinders can be seen lying parallel to the film surface, with an intercylinder spacing of ~27 nm. At 1 kV, the sampling depth is sufficiently shallow that we are imaging the topmost layer of cylinders without a significant contribution from the lower layer of cylinders, as will be discussed further in a following section. The etching depth can be controlled to within a few nanometers by the time per etching step. This would allow one to examine smaller microstructures in other systems. The film roughness created by this process has a length scale of only a few nanometers, as determined by high resolution TEM work, and is not detrimental to obtaining high quality SEM images. In addition, we find this roughness to be non-cumulative for deeper etches, as will be discussed in a following section.

From the set of images of *Figure 1*, we can estimate the SEM depth resolution, or the minimum resolvable distance between imaging planes, at an incident beam voltage of 1 kV. Since etching away 7 nm allowed us to barely observe the cylinders that we found to be unobservable at 15 nm beneath the surface, we estimate the SEM depth resolution to be 10 nm. Because the resolution of this technique is twice as fine as the interlayer spacing, we can truly obtain layer by layer imaging rather than a two-dimensional projection.

THE EFFECT OF THE SEM OPERATING VOLTAGE ON THE IMAGE SAMPLING DEPTH

The operating voltage of the SEM can be varied to select the electron penetration depth into the sample, and hence the depth from which the signal emerges, which we shall refer to as the sampling depth[12]. For block copolymer microstructures, this quantity changes remarkably over the voltage range of 1–4 kV. We have demonstrated this by imaging the topmost layer of a stained SB 36/11 bilayer on a silicon wafer, from the same set of samples as used in the previous section. However, instead of etching the sample as in the previous section, we have varied the operating voltage. To minimise any potential variation of the resolution of the SEM, all measurements were made within a 3-h period on the same SEM. In addition, it is known that the lateral resolution of a SEM decreases with decreasing voltage, but in our studies, we found the decrease in resolution between 1 and 4 kV was not significant. We

present images (*Figure 3*) at each operating voltage which represent the typical contrast that was observed. The images were obtained from the same sample, but not from the same location in the sample.

At 1 kV, the SEM is merely imaging the wetting layer of PB, as can be seen in *Figure 3a*, consistent with our results in *Figure 1a*. The sampling depth must be less than 15 nm since the cylinders are ~15 nm beneath the sample surface. As we increase the voltage to 2 kV to increase our sampling depth, we can begin to see the cylindrical microstructures, though the contrast is poor (*Figure 3b*). Increasing the operating voltage to 3 kV increased the contrast (*Figure 3c*). The contrast appeared to be optimised at 4 kV (*Figure 4d*), for increasing the voltage to 5 kV and higher resulted in no significant increase in contrast. Since the cylindrical microstructures are submerged ~15 nm beneath the surface wetting layer of PB, the sampling depth must be greater than 15 nm at voltages above 2 kV.

We have demonstrated that the sampling depth can be set with surprising sensitivity via the operating voltage. To illustrate the usefulness of controlling the sampling depth, we use a stained film of SI 68/12 which formed regions§ of PI sphere bilayers next to regions of sphere monolayers.¶ As described in a previous section, we used a RIE to etch away the PI wetting layer and the PS matrix closest to the surface (20 nm of film was etched away) to expose the top layer of spheres to the surface for imaging. The films shown in *Figure 4* consist of a bilayer of spheres on the left side and a monolayer of spheres on the right side, determined by locally measuring the film thickness with an interferometer. A dashed line is used to separate the bilayer region from the monolayer region. At 1 kV we set a shallow sampling depth and image only the top layer of spheres in the bilayer (left side) or monolayer (right side) in *Figure 4a*. At 3 kV, the sampling depth is large enough to image both the top and bottom layers of spheres, as shown in *Figure 4b*. The monolayer of spheres on the right side of *Figure 4b* produces an image free of superposition effects. However, on the left side of *Figure 4b*, the bilayer produces a superposition pattern of the two overlapping layers of spheres. In many regions, one sees black dots on a white background, a reversal of the contrast observed from the monolayer of spheres. The offset of the top and bottom layer of spheres produces these Moiré-like regions of contrast reversal. The microstructure layer closest to the surface appears slightly brighter than the layer underneath due to the higher electron production of structures closer to the surface. Though we have imaged two layers simultaneously at 3 kV, increasing the sampling voltage further is not effective for imaging more than two layers of microstructures, for the greater the number of layers imaged simultaneously, the more difficult the interpretation of the image.

Judging from the contrast of the images presented, we suggest that that by selecting operating voltages greater than 1 kV, one can image effectively image microstructures that are submerged up to ≈ 30 nm, the inter-layer spacing of the spheres inside the polymer film of *Figure 4*. Ideally, one etches with an RIE to expose the desired microstructures to the surface and sets the sampling depth to be approximately the microstructure thickness, typically 10 nm at 1 kV. We find that this technique produces the images with the greatest contrast and resolution. By repeating this process, we have depth profiled thicker films, as will be discussed in a following section.

§ Islands formed on the film surface from spin coating the film at a thickness incommensurate with an integral number of spherical layers. This is more fully described in a following section.

¶ This sample was annealed at 200°C, but similar samples annealed at 130°C displayed consistent results.

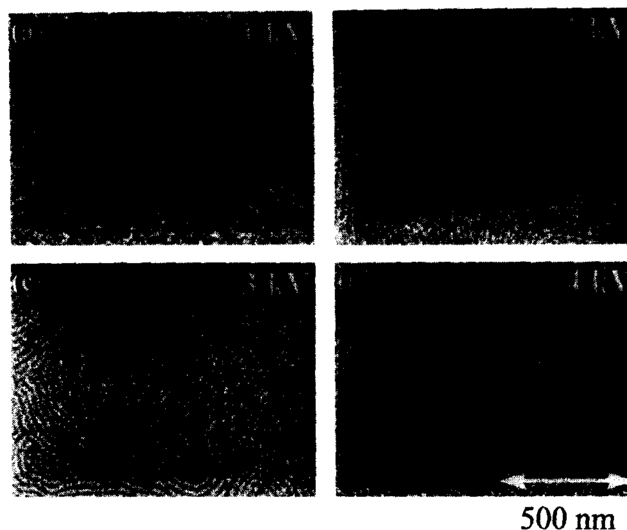

Figure 3 By increasing the SEM operating voltage from 1 to 4 kV, we have increased the sampling depth and we can image the internal microstructures through the PB surface wetting layer without etching. These images do not correspond to the same location on the film surface.

COMPARISON OF O_2 ETCHING TO CF_4 ETCHING FOR SEM ANALYSIS

O_2 plasma etching is more typically used for etching polymer films for SEM analysis. In a plasma etcher, the sample is placed directly in the electrically neutral plasma and bombarded by ions and neutrals at a much lower energy than in a reactive ion etcher, in which the sample is typically placed on a cathode which is at a negative voltage with respect to the plasma (*Figure 2*). The etching rate of a polymer in a plasma etcher is strongly dependent on the polymer's molecular composition since the etching is achieved mainly due to chemical reaction. For example, PI etches 5 times as quickly as PS under oxygen plasma etching[18]. As a comparison, our technique relies upon the non-selectivity of CF_4 RIE. Other groups have investigated O_2 plasma etching for SEM analysis of polymer microstructures[19,20]. Nishimura *et al.* used an oxygen plasma etching system which selectively removed polymer material in order to image internal glass fibers imbedded in a polymer matrix. In this case, they were relying on the O_2 plasma etching selectivity between glass and polymer, or in other cases, the etching selectivity between polymer microstructures imbedded in a matrix of a different polymer composition. Their technique was adequate for imaging the top layer of the structures, but as acknowledged by the authors, additional etching increased the density of non-etchable microstructures on the surface, preventing effective depth profiling.

In addition to O_2 plasma etching, O_2 reactive ion etching is commonly used to etch polymer films. As a comparison to CF_4 RIE, we investigated O_2 RIE with similar power and pressure conditions and found that the etch rate of PB is 33% higher than the etch rate of PS. Though not as pronounced as the difference in etch rates observed with O_2 plasma etching, this difference would prevent effective depth profiling for PS-PB films. In addition, O_2 RIE

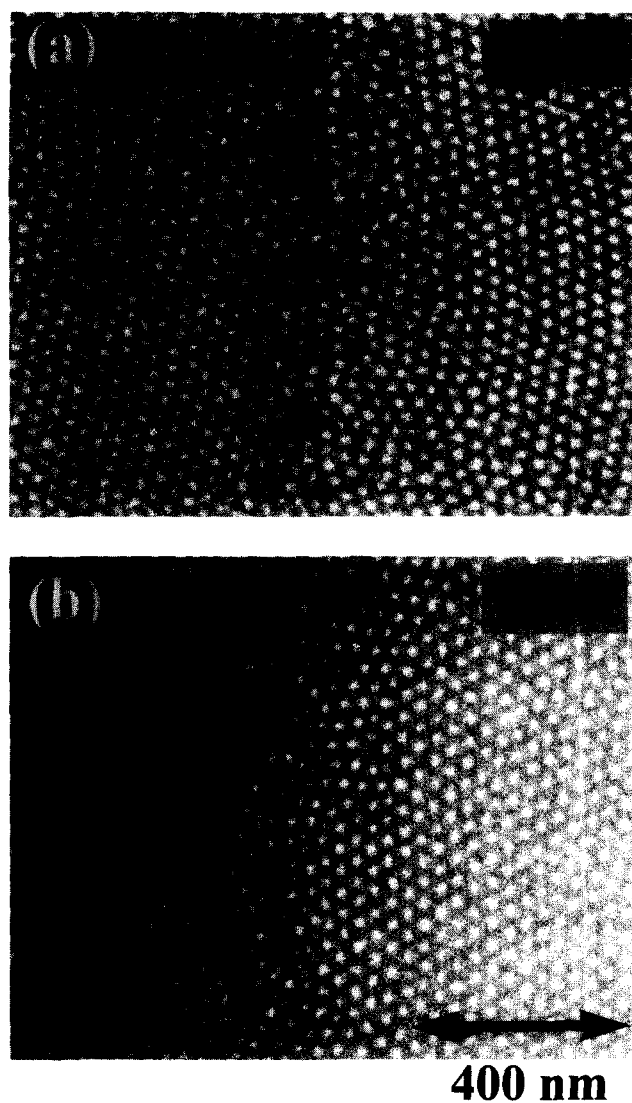

Figure 4 In both images, there is a bilayer of spheres on the left side of the image and a monolayer of spheres on the right side of the image. These films have been etched with CF_4 RIE to expose the PI spheres to the surface. (a) At 1 kV, we only see the top layer of spheres for the bilayer (left side) and the monolayer (right side). (b) At 3 kV, the greater sampling depth allows us to image the superposition of the top and the bottom layer on the left, and clearly image the single layer on the right.

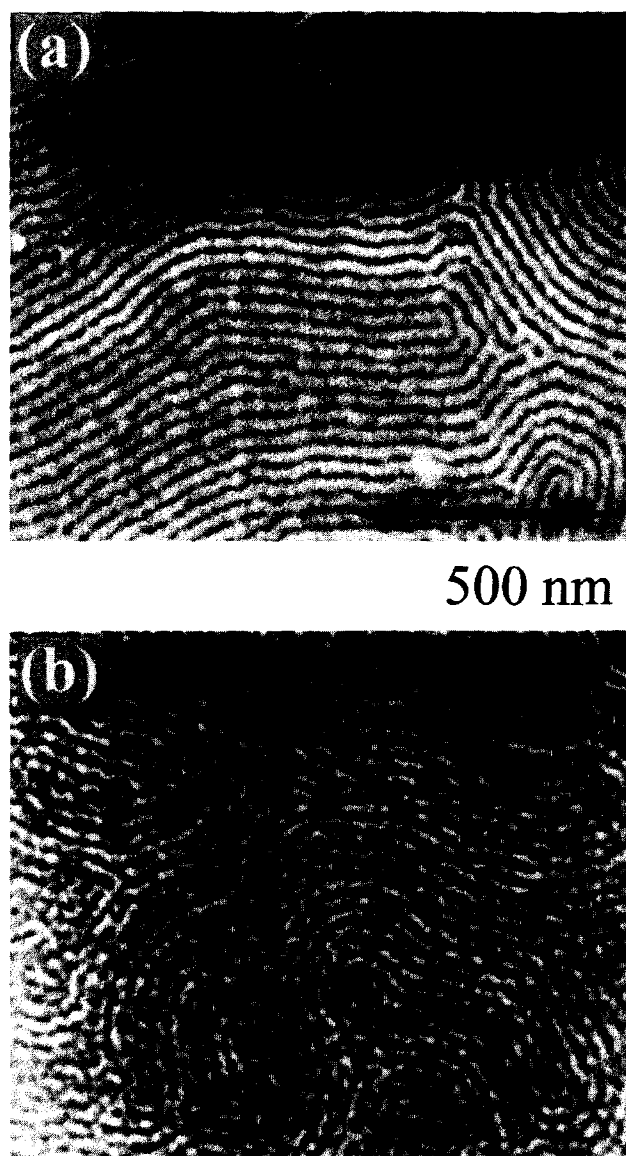

Figure 5 (a) After etching the ozonated cylinder monolayer with CF_4 RIE, we see a high resolution image of the cylindrical voids (dark) and the PS matrix (light). (b) With similar conditions for O_2 RIE, we see the sample surface has been damaged with holes (10 nm wide randomly distributed dark spots). (SEM voltage: 1 kV)

produces a roughness with a length scale of 10 nm on the film's surface which could be confused with the actual morphology. This roughness is shown in the comparison of *Figure 5a* and *b*. For these images, we have taken monolayer polymer films of SB 36/11 (the same polymer as used above), removed the PB domains with ozone, and then etched with CF_4 RIE (*Figure 5a*) and O_2 RIE (*Figure 5b*) to expose the trough-like voids to the surface by etching away the top ~15 nm of polymer film. The film etched with CF_4 appears to be smoothly etched without any artifacts, where the dark regions correspond to the voids left by the ozonation of cylindrical PB domains and the light regions correspond to the PS matrix. The film etched with O_2, however, is significantly roughened, as can be seen by the dark pits left throughout the image. We also observed a roughening of similarly prepared homopolymer PS films with O_2 RIE. Others have reported a roughening of polymer surfaces with O_2 RIE compared to CF_4 RIE, but it is still unclear as to how O_2 RIE roughens the surface whereas CF_4 RIE etches smoothly[21]. Hence we do not recommend O_2 RIE as a means of smoothly etching polymer surfaces. In addition, argon ion milling of these samples was attempted, but the resulting samples were so damaged that the image quality was insufficient for imaging the microstructures.

MORPHOLOGY OF 1ST AND 0TH LAYERS

The optimal thickness for producing a monolayer of cylinders of SB 36/11 on a silicon wafer is 50 nm, which is approximately twice the interlayer spacing of the microstructures. This extra thickness is accounted for by the PB wetting layers on the top and bottom of the film. We shall refer to this monolayer of cylinders, including the wetting layers, as the 1st layer, represented schematically in *Figure 6a*. By spin coating polymer films, we can obtain a film thickness which is uniform within a few percent across the entire silicon wafer. Monolayers of cylinders of SB 36/11 were examined by SEM after staining and etching away the PB surface layer. A typical image is shown in *Figure 6b*

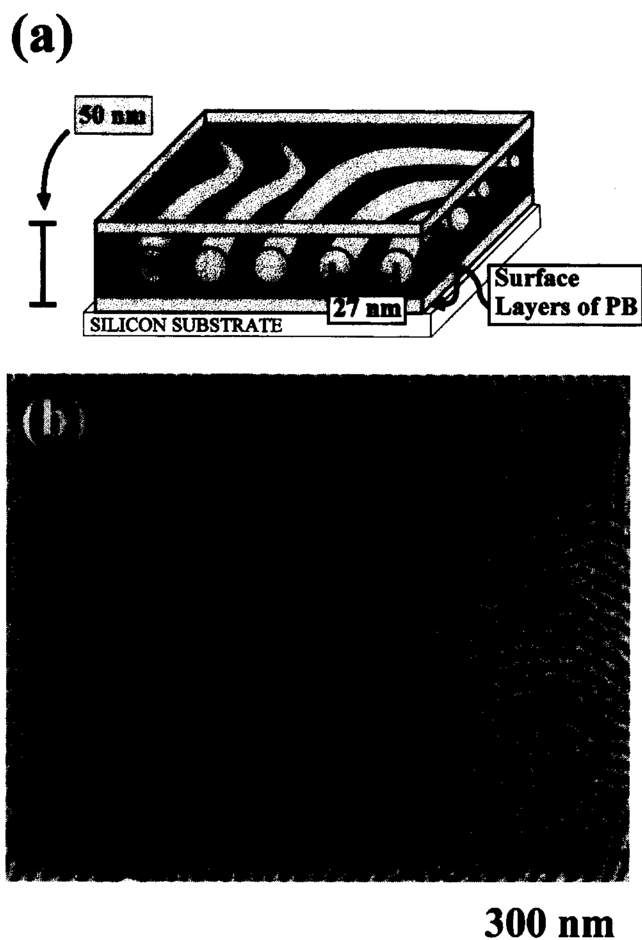

Figure 6 (a) Schematic of one monolayer of PB cylinders on a silicon substrate. We have determined from secondary ion mass spectrometry data that there is a wetting layer of PB at the free interface and also on the silicon substrate. (b) SEM image obtained from a monolayer of cylinders on a substrate. There are cylinders lying predominantly parallel to the film surface and isolated spheres. (SEM voltage: 1 kV)

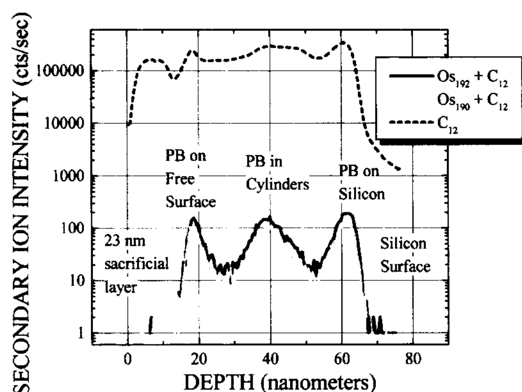

Figure 7 SIMS data from a monolayer of cylinders such as shown in Figure 6. There are three peaks in the traces of the osmium-carbon compounds, which correspond to the PB density. The peak at 18 nm corresponds to PB wetting the free surface of the copolymer film, the peak at 40 nm corresponds to the PB rich microstructure domains, and the peak at 65 nm corresponds to the PB wetting layer on the silicon surface.

which shows a predominant morphology of cylinders lying parallel to the substrate.

We have determined by dynamic Secondary Ion Mass Spectrometry (SIMS) that there is a wetting layer of PB at both the free surface[22] and the silicon–polymer interface, as shown in *Figure 7*. For SIMS analysis, samples were prepared as previously described, including annealing and staining. To track the stained PB concentration, the signals of two osmium isotopes (isotopes 190 and 192, whose relative abundance in the sample correlated with their natural abundance) in carbon compounds were monitored in the secondary ions. The masses of the osmium–carbon compounds were 202 and 204 amu. The decrease in the carbon signal was used to mark the copolymer–silicon interface. The data show three peaks in osmium yield: the first peak from the PB-rich free surface, the next peak from the PB microstructures, and the last peak from the PB-rich copolymer–silicon interface.

The free surface of the copolymer film is wet by PB, the lower surface tension component. However, the wetting of the native oxide of the silicon surface by PB is more difficult to interpret, because we must consider the interfacial tension between each block and the polar native oxide. It has been shown by others that the interfacial tension between hydrocarbon chains and water, a polar fluid, strongly depends upon the level of unsaturation[23]. For a completely saturated alkane chain of 10 carbons, an interfacial tension of 52 mJ/m^2 was measured. For a similar alkene chain with one unsaturated C–C bond, the interfacial tension dropped to 19 mJ/m^2, showing the strong effect of the C=C double bond on reducing the interfacial tension. In addition, the interfacial tension betwen benzene, an aromatic hydrocarbon as is PS, and water was measured to be 35 mJ/m^2. Therefore, we suggest that the interfacial tension between unsaturated hydrocarbons such as PB and a polar surface, such as the native oxide of silicon, will be lower than that of an aromatic hydrocarbon such as PS with a polar surface. In addition, as has been pointed out by others[24,25] and confirmed by experiments of our own, PB exhibits a strong interaction with silicon and silicon oxide substrates, as can be demonstrated by attaching PB homopolymers to silicon wafers (which have native oxides) by spin coating and annealing. This may be caused by the formation of chemical bonds between the PB and the silicon substrate.

Up to this point, the SEM images presented have shown a continuous film containing microstructures throughout the image. However, not all spin coated films contain such uniform microphase separation. The microphase separation of a block copolymer results in quantised film thicknesses which depend on the number of microstructure layers which self-assemble internally. If a film is spin coated slightly thicker than needed to form n monolayers of microstructures, this thickness constraint (in conjunction with conservation of polymer mass) forces 'islands' of $n + 1$ layers to form on top of a uniform film of n layers. Conversely, if a film is spin coated slightly thinner than needed to form n monolayers of microstructures, this constraint produces 'holes', which are regions of $n-1$ layers in a thicker background of n monolayers[26].

If the polymer film is on a reflective substrate, such as silicon, the micron-size holes or islands can easily be seen with a high quality optical microscope since the interference colour of a region depends upon the film thickness. An interferometer attached to an optical microscope can quickly (1 min) measure the film thickness (± 2 nm) in an area as small as 2 μm^2, appropriate for locally measuring the thickness of an island or hole. One of the advantages of imaging polymer microstructures with this RIE/SEM technique is that one can measure the film thickness with an interferometer in a certain region and then directly image the microstructure in the same region to study the effect of film thickness on the microstructure. In typical TEM use,

absolute thickness measurements are difficult to obtain. Relative thickness measurements by densitometry are possible but require a calculation which depends upon the internal morphology of the film's internal microstructure and an independent thickness measurement determined by an interferometer or an ellipsometer. In addition, careful photographic work to calibrate a response curve of the plates for each developed batch is necessary to obtain accurate measurements[27].

The techniques that we have developed can be used to study copolymer islands and holes and how they affect the morphology. If we spin coat an SB 36/11 copolymer film at an average thickness of 40 nm, less than that of a monolayer of the 1st layer (50 nm), holes (0th layer) develop during annealing. By interferometry, we have measured the thickness of the thicker regions outside of the holes of the film (1st layer) to be ~50 nm and the thickness of thinner regions (in the holes) of the polymer film to be about 30 nm (0th layer). We refer to this thinner layer as the 0th layer because of the absence of internal microstructures, as will be shown. A typical image of the copolymer film with a hole is shown in *Figure 8* where we have stained the film and removed the top 12 nm for optimal imaging as described

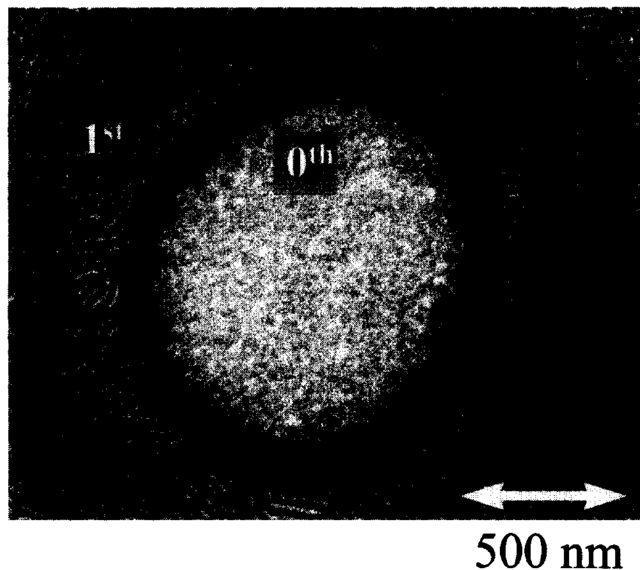

Figure 8 A hole forming in a film of a monolayer of PB cylinders, SB 36/11. The stained PB microstructures appear light in the SEM image. There are spheres in the region between the 1st and 0th layers. This morphological change is caused by the gradual decrease in thickness from the thicker 1st layer to the thinner 0th layer, producing an effectively lower PB volume fraction in this region.

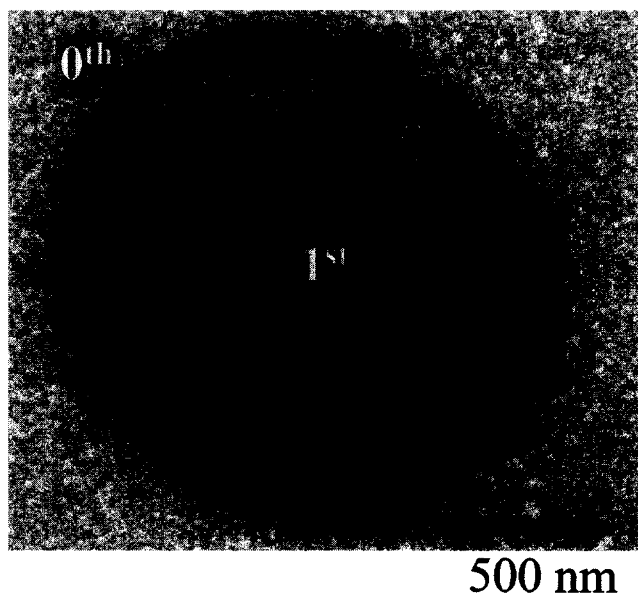

Figure 9 An isolated island of cylinders forming on a film of SB 36/11. The stained PB cylinders appear light in the SEM image. The decrease in thickness from the 1st layer to the 0th layer produces a morphology of hexagonally packed spheres.

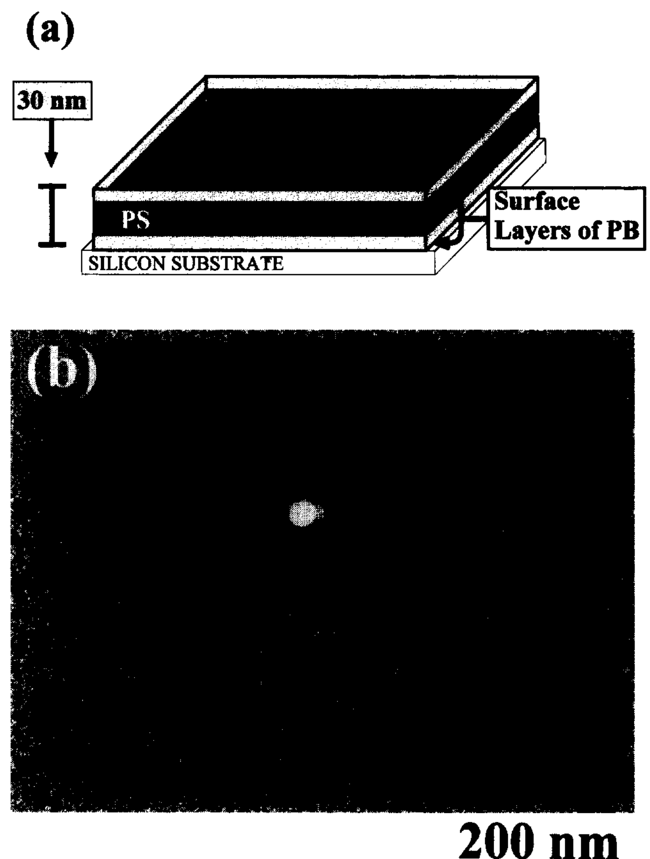

Figure 10 (a) Schematic of the 0th layer on silicon. PB wets the copolymer free surface and the copolymer-silicon interface, isolating the PS. (b) SEM image of the 0th layer, showing the lack of microstructures. A gold sphere that can be seen in the middle of the image establishes that we are imaging the polymer surface with sufficient resolution. (SEM voltage: 1 kV)

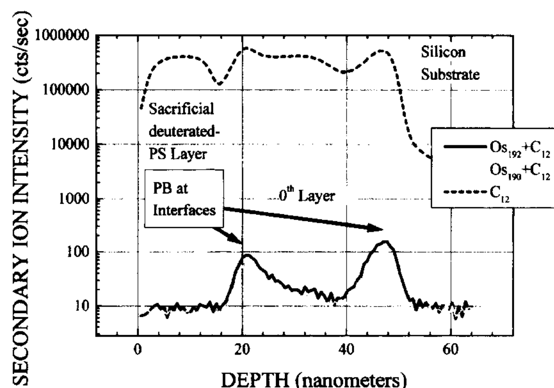

Figure 11 SIMS data from the 0th layer on silicon. A decrease in the C_{12} yield marks the copolymer-silicon interface. The two peaks in osmium yield correspond to the PB-rich wetting layers on the copolymer free surface and the copolymer-silicon surface, as drawn in Figure 10(a).

previously. The bulk morphology of cylinders is seen in the thicker 1st layer surrounding the hole, but along the edge of the hole, a morphological transition to spheres is typically seen. In the 0th layer region, no microstructures can be observed.

By spin coating at an average thickness of 35 nm, a morphology of isolated round islands of microstructures develops during annealing (*Figure 9*). Again, we see cylinders (the bulk morphology) in the interior of the thicker region of the island (1st layer) and hexagonally packed spheres on the periphery. Off of the island, no microstructures are observed in the 0th layer. In both the images of the hole and the island (*Figure 8* and *Figure 9*), the morphological transition from cylinders to spheres can be seen in the regions where the film thickness is between that of the 1st and 0th layers. We suggest that in these regions, the PB wetting layers are depleting the available PB for the microstructures and driving the morphology to an effectively lower PB volume fraction, producing spheres[5]. We are currently working on a larger study of this morphological transition.

By spin coating films of 30 nm thickness, we can make a uniform film of the 0th layer, without formation of islands or holes. As was determined by SIMS analysis, this 0th layer is composed of PB wetting layers on the free and confined surfaces (*Figure 10a*) without internal microstructures, as shown by SEM using the RIE/SEM technique (*Figure 10b*). This lack of microstructures was confirmed by TEM analysis. Samples of the uniform 0th layer were prepared for SIMS analysis (*Figure 11*) as described previously. The decrease in the carbon yield was used to determine the copolymer–silicon interface. We can see osmium-intense peaks associated with PB wetting the free surface and the copolymer–silicon interface. However, there is no peak between these two, indicating the absence of internal microstructures, verifying our observations with the SEM.

In addition, we examined thin polymer films of SB 65/10 on a silicon wafer, spin coated and prepared in a similar manner to the films of SB 36/11 discussed earlier in this section. The diblock copolymer SB 65/10 produces spheres of PB in a matrix of PS, which we imaged using the RIE/SEM technique. Once more, to obtain these images, it was necessary to stain the PB domains with osmium tetraoxide in order to provide SEM contrast between the PB and PS and to etch away the surface layer of PB with a RIE. *Figure 12* shows SEM images of the SB 65/10 polymer film spin coated at a thickness slightly less than needed for

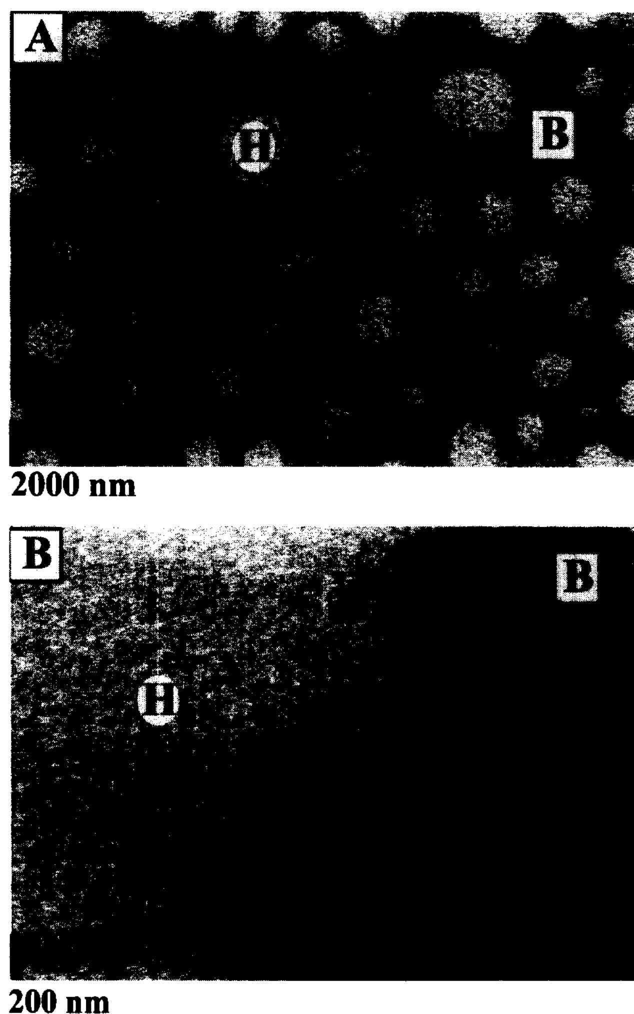

Figure 12 (a) Low magnification SEM image of holes (lighter regions, ~30 nm thick) in a film of SB 65/10. The letter H corresponds to a hole. The darker regions marked B correspond to a thicker background (~60 nm) which contains one monolayer of well-ordered PB spheres. (b) High magnification SEM image at the boundary of a hole. At this magnification, the microstructures are observable in the thicker region. Both SEM images are obtained at 1 kV.

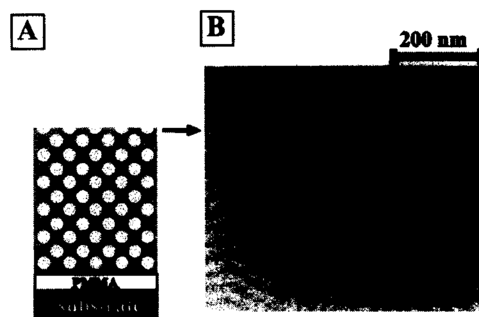

Figure 13 (a) Cross sectional schematic of a cylindrical diblock copolymer (SB 36/11) film on a PMMA-coated substrate, about 11 cylinder layers thick (240 nm). The lighter regions are the cylinders of PB which are oriented perpendicular to the page and parallel to the substrate. We have stripped off the top 12 nm to obtain an SEM image of the layer of cylinders closest to the surface. (b) SEM image of the surface of the etched diblock copolymer film as shown in (a). SEs from below the top layer of cylinders cannot escape to be detected, producing an image of the top monolayer. (SEM voltage: 1 kV)

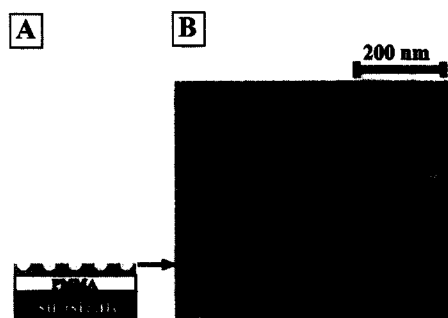

Figure 14 (a) Cross sectional schematic of a cylindrical diblock copolymer (SB 36/11) on a PMMA-coated substrate. The lighter regions are the PB cylinders which are oriented perpendicular to the page, but parallel to the substrate. The initial SB 36/11 film thickness was 240 nm, but after etching away 200 nm with a RIE, the thickness is 40 nm, which leaves one monolayer of cylinders on the surface. We can now image the layer closest to the bottom since its cylinders are exposed on the surface. (b) SEM image of the sample shown in (a). (SEM voltage: 1 kV)

complete coverage by one monolayer of PB spheres. The low magnification SEM image (*Figure 12a*) shows light regions corresponding to holes (0th layer of ~30 nm thickness, labelled H) and dark regions corresponding to the thicker continuous polymer background (1st layer of ~60 nm thickness, labelled B). The thinner regions appear bright due to an increased electron yield from the silicon substrate which can increase the SE yield (see 'Contrast Mechanism' section). Upon examination at a higher magnification (*Figure 12b*), the thicker background region shows well-ordered spherical microstructures while the thinner holes do not display any microstructures. Since the same wetting phenomena will affect the morphology of SB 65/10 films as SB 36/11 films, the region of the 0th layer holes seen in SB 65/10 will be composed of PB wetting the free and confined surface with a PS matrix inside (as shown in *Figure 10* for SB 36/11).

SEM DEPTH PROFILING

In addition to imaging the microstructures in monolayers of cylinders or spheres in thin films, this technique allows us to examine the morphology in thick films (several monolayers) as a function of depth. If we wish to obtain an image of the layer which is underneath, we simply remove the layer on the surface by further etching of the polymer film and subsequently examine the newly exposed layer by SEM. By alternating between examining a monolayer with SEM, removing it by RIE, and further SEM examination of the layer underneath, we can obtain images of the microstructures as a function of depth.

An example of depth profiling is shown in *Figure 13* and *Figure 14*. In this case, the initial film thickness of SB 36/11 was 240 nm, about 11 layers of cylinders. This polymer film was spin coated on a silicon wafer which was previously coated with a 130-nm thick layer of PMMA (as described in the 'Sample preparation' section). Similar depth profiling studies with SB 36/11 on bare silicon substrates yield consistent results to those presented in *Figure 13* and 14 with PMMA precoated substrates. First, we examined the layer of cylinders which is closest to the top surface (*Figure 13*). As previously described, we etched away the PB outer layer to obtain this SEM image. Next, we alternated between stripping off a layer of cylinders and examining the exposed monolayer by SEM. After removing 200 nm of polymer film by RIE, there was a thickness of only one monolayer of cylinders remaining on the substrate (~40 nm). An image of this specimen is shown in *Figure 14*. For the images presented in *Figure 13* and *Figure 14*, we have not examined layers which were directly underneath one another. However, at each depth that was examined, the orientation of the cylinders was predominantly parallel to the film surface, suggesting that the surfaces can influence the orientation of the microstructures that are up to five inter-cylinder distances away.

In *Figure 13* and *Figure 14*, we demonstrate that we can remove tenth-micron film thicknesses without creating significant cumulative roughness and damage to the remainder of the film. If the etching process were to introduce significant sample roughness, then we would be unable to etch 200 nm into the polymer film without obscuring the image of the cylinder microdomain structures. *Figure 14* shows that the quality of the image after a 200-nm etch is comparable to the image obtained after the initial 12-nm etch.

If the film consists of two or more monolayers of cylinders (and is not on a substrate), then TEM will image a projection of the layers in the film. The advantage of using SEM is that we can image each monolayer separately, for the sampling depth of the SE at 1 kV is less than the interlayer spacing of the cylinders. In order to obtain comparable depth information to that shown in *Figure 13* and 14 via TEM, microtoming would be required to cut cross-sectional slices of a sample. Microtoming, by its nature, can introduce distortion in the film during cutting and has a thickness resolution of approximately 70 nm, several times the periodicity of typical microstructures. Furthermore, it is difficult to successfully microtome a cross-section of a soft polymer film on a hard substrate such as a silicon wafer due to the large mismatch in hardness between the two materials. Lastly, microtomed sections represent only a slice of the film which is not necessarily characteristic of the sample, while this RIE/SEM technique allows one to image the entire film area at any depth. Therefore, this RIE/SEM technique provides a complementary method to obtain cross-sectional information of films on various substrates.

By successive iterations of this RIE/SEM technique, a three-dimensional map of the sample could be obtained. To examine the microdomain layer which is directly underneath a region currently being examined, it would be necessary to have an alignment mark in the sample such that the same lateral location could be imaged during depth profiling. An alignment mark could be a natural landmark such as a spin coat defect or an intentionally created structure. We find that a few scribe lines suffice. By alternating between SEM and RIE, one can study, for example, the propagation of defects and domain orientations through the sample. To our knowledge, we know of no other technique (besides microtoming) that can obtain depth information of bulk samples with sufficient lateral resolution to directly image block copolymer microstructures.

In order to depth profile a diblock copolymer system with this RIE/SEM technique, it is important that the two blocks

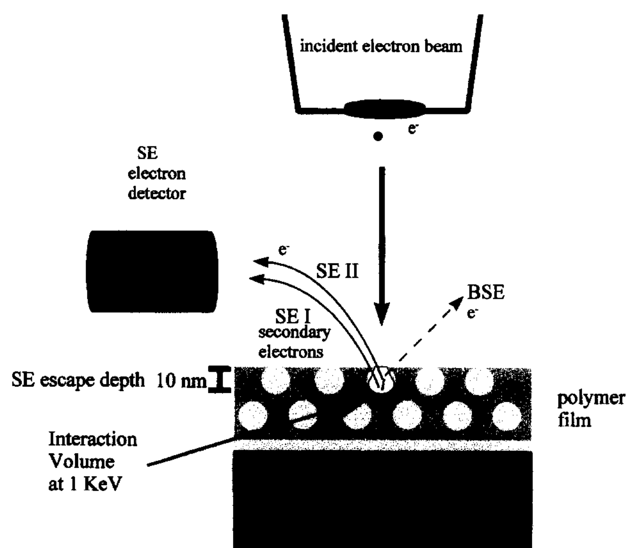

Figure 15 Schematic of the interaction of an incident electron beam (1 kV) with a two monolayer thick polymer sample. SE I are produced by direct interaction of the incident beam with the sample. The dashed line shows the interaction of a BSE electron with the sample to produce an SE II. The increase in BSE yield in stained PB domains increases the SE II yield in those regions to provide SE chemical composition contrast.

etch at approximately the same rate. Otherwise, the microdomain structure will quickly be lost due to topography introduced by selective etching, obscuring the image. By choosing an appropriate RIE gas which etches both blocks at the same rate, other diblock copolymer systems could be examined in a similar manner. Others have shown that polymers with quite different chemical compositions such as polyimide and polyethylene have similar etch rates under CF_4 RIE[28], so we expect that this technique could be applied to depth profile a variety of block copolymers. It is important that the microdomain structures not be altered during the etching process, which can heat the system above their glass transition temperature (T_g) and increase the mobility of the polymer chains. To avoid altering the microstructures during etching, the diblock copolymer system can be cross-linked or kept below T_g of one of the blocks during the etching process. The latter can be accomplished by placing the sample on a cooling stage in the RIE or by alternating between short etches and sufficient cooling periods.

CONTRAST MECHANISM

As mentioned previously, we find suitable SE or BSE contrast between the PS domains and the stained PB or PI domains. Etching with a RIE does not produce significant topographical features and the contrast between the domains is primarily due to chemical variation (from the OsO_4 staining). In typical SEM use with a high energy electron beam, BSE rather than SE are collected to obtain chemical composition contrast due to the much higher atomic number dependence of BSE yield compared to SE yield. However, in order to maximise contrast and to minimise charging effects in our non-conducting polymer samples, we used a low energy incident beam where we found sufficient contrast between PS and stained PB or PI using either SE or BSE, though the SE resolution was slightly higher than the BSE resolution.

At low beam energy, the chemical composition contrast of the SE signal is due to its contribution from the BSE yield's atomic number dependence. In an SEM, SE ($\sim < 50$ eV) are produced by ionisation of atoms by the electron beam, whereas BSE (> 50 eV) are produced by high angle elastic scattering. Within a few nanometers of the point of impact, scattering of the primary electron beam produces both BSE I and SE I. Back-scattered electrons are also produced at greater distances from the point of impact, denoted BSE II, and can create a cascade of secondary electrons, denoted SE II (*Figure 15*). The SE contrast is produced by the sum of both SE I and SE II. At low energy, the interaction volume of the incident beam is small enough that the SE II signal does not cause a significant decrease in resolution, as is the case for the SE II produced with high energy incident electrons[10].

It has been shown at incident beam energies of 25 keV that the SE I yield is not strongly atomic number dependent[29] (we roughly estimate less than 10% difference between carbon and osmium), which we extrapolate to the low energy regime. However, the SE II yield is dependent on atomic number because of their production by BSE II. It is well-known that the BSE yield rises monotonically with atomic number when the incident electron energy is around 25 keV[29], and recently it has been shown at low energies around 1 keV that the BSE yield also rises substantially with atomic number[30]. The BSE yield at low energies increases by approximately a factor of eight from carbon (atomic number 6) to osmium (atomic number 76). In agreement with these recent findings, we observe satisfactory BSE imaging contrast with the higher BSE yield of OsO_4 stained domains as compared to the PS matrix. This modulation in BSE yield produces a modulation in the SE II yield[31] to provide SE contrast (in addition to BSE contrast) between the PS domains and the OsO_4-stained PB domains.

This model of BSE II production of SE II to provide SE contrast is in agreement with our study of the effect of the operating voltage on the sampling depth. In a previous section, we showed that cylinder microstructures could be imaged through the PB wetting layer (without RIE) by choosing a high enough incident beam energy (*Figure 3*). It has been shown that the electron range[12] in the sample increases with voltage to the 5/3 power, which we used to increase our sampling depth. Though the cylinders were submerged below the ~ 15 nm depth from which SE I could originate, sufficient contrast with the total SE signal was still seen, suggesting that the SE II strongly contribute to the observed contrast. At the sufficiently deep electron range selected at 4 kV, the incident beam reached the cylinders and produced BSE II in the submerged cylinders. These BSE scatter at high angles and exit the sample through the top surface, producing a cascade of SE II close to the surface which become part of the observed contrast in the SE signal.

CONCLUSIONS

We have shown that the microstructure of PS–PB and PS–PI diblock copolymer films can be successfully imaged with a technique that combines RIE and low voltage, high resolution SEM. This technique is relatively simple, requiring only an RIE and some means of measuring the film thickness such as an ellipsometer or an interferometer to calibrate the etching rate. An RIE with CF_4 gas at low energy and with the parameters specified in this paper etches OsO_4-stained PS–PB polymer films non-selectively, uniformly and in a controlled manner. By proper choice of the RIE gas and parameters this technique can be applied to other block copolymer systems. This RIE/SEM technique is a supplement to microtoming and a useful tool for researchers examining block copolymers on substrates.

ACKNOWLEDGEMENTS

We would like to thank the staff of the Cornell Nanofabrication Facility for their assistance with using their instruments. In addition, this project was greatly assisted by the facilities of the Advanced Technology Centre for Photonics and Optoelectronic Materials (ATC/POEM) of Princeton University and the Princeton Materials Institute. Also, we thank the Centre for Ceramics Research at Rutgers University for allowing us to use their SEM. We would like to thank Charles Magee and staff at Evans East, Inc., for SIMS analysis. We acknowledge helpful discussions with Prof. Michael S. Isaacson.

REFERENCES

1. Bates, F. S. and Fredrickson, G. H., *Ann. Rev. Phys. Chem.*, 1990, **41**, 525.
2. Henkee, C. S., Thomas, E. L. and Fetters, L. J., *J. Mater. Sci.*, 1988, **23**, 1685.

3. Anastasiadis, S. H., Russell, T. P., Satija, S. K. and Majkrzak, C. F., *Phys. Rev. Lett.*, 1989, **62**, 1852.
4. Mansky, P. and Russell, T. P., *Macromolecules*, 1995, **28**, 8092.
5. Park, M., Harrison, C., Chaikin, P. M., Register, R., Adamson, D. and Yao, N., *Morphological Control in Multiphase Polymer Mixtures*, Vol. 461. Materials Research Society, Boston, MA, 2–6 December 1996 (Materials Research Society, Pittsburgh, PA, 1997), pp. 179–184.
6. Radzilowski, L. H., Carvalho, B. L. and Thomas, E. L., *J. Polym. Sci. B*, 1996, **34**, 3081.
7. Spontak, R. J., Fung, J. C., Braunfeld, M. B., Sedat, J. W., Agard, D. A., Kane, L., Smith, S. D., Satkowski, M. M., Ashraf, A., Hadjuk, D. A. and Gruner, S. M., *Macromolecules*, 1996, **29**, 4494.
8. Park, M., Harrison, C., Chaikin, P. M., Register, R. and Adamson D., *Science*, 1997, **276**, 1401.
9. Morkved, T. L., Lu, M., Urbas, A. M., Ehrichs, E. E., Jaeger, H. M., Mansky, P. and Russell, T. P., *Science*, 1996, **273**, 931.
10. Thomas, E. L., Vezie, D. L. and Adams, W. W., *Polymer*, 1995, **36**, 1761.
11. Butler, J. H., Joy, D. C., Bradley, G. F. and Krause, S. J., *Polymer*, 1995, **36**, 1781.
12. Joy, D. C. and Joy, C. S., *Micron*, 1996, **27**, 247.
13. Brostin, J., *Scanning*, 1995, **17**, 329.
14. Lai, Q. J., Simmons, S. R., Albrecht, R. M. and Cooper, S. L., *ACS PMSE Proc.*, 1992, **66**, 28.
15. Morton, M. and Fetters, L. J., *Rubber Chem. Technol.*, 1975, **48**, 359.
16. Mansky, P., Harrison, C. K., Chaikin, P. M., Register, R. A. and Yao, N., *Appl. Phys. Lett.*, 1996, **68**, 2586.
17. A good introduction to RIE is given by van Roosmalen, A. J., Baggerman, J. A. G., Brader, S. J. H., *Dry Etching for VLSI*. Plenum Press, New York, 1991.
18. Taylor, G. and Wolf, T., *Polym. Eng. Sci.*, 1980, **20**, 1087.
19. Ramesh, N. S., Padiyath, R., Campbell, G. A. and Babu, S. V., *J. Polym. Sci. B*, 1991, **29**, 1031.
20. Nishimura, H., Yarita, T. and Noshiro, M., *Reports Res. Lab. Asahi Glass Co. Ltd.*, 1983, **33**, 151.
21. Egitto, F. D., Matienzo, L. J. and Schreyer, H. B., *J. Vac. Sci. Technol. A*, 1992, **10**, 3060.
22. The PB at the free surface layer has been previously observed by Hashimoto, T. Hasegawa, H., *Polymer*, 1992, **33**, 475.
23. Israelachvili, J., *Intermolecular and Surface Forces*. Academic Press, San Diego, CA, 1992, p. 315.
24. Ahagon, A. and Gent, A. N., *J. Polym. Sci., Polym. Phys. Ed.*, 1975, **13**, 1285.
25. Jones, R. A. L., Norton, L. J., Shull, K. R., Kramer, E. J., Felcher, G. P., Karim, A. and Fetters, L. J., *Macromolecules*, 1992, **25**, 2539.
26. Coulon, G., Ausserre, D. and Russell, T. P., *J. Phys. France*, 1990, **51**, 777.
27. Lauterwasser, B. D. and Kramer, E., *J. Philosophical Magazine A*, 1979, **39**, 469.
28. Cain, S. R., Egitto, F. D. and Emmi, F., *J. Vac. Sci. Technol. A*, 1987, **5**, 1578.
29. Reimer, L., *Scanning Electron Microscopy*. Springer, New York, 1995, p. 136.
30. Hejna, J., *Scanning*, 1995, **17**, 388.
31. Lin, P. and Crew, A., *Proc of the 1975 Elect. Micro. Soc. of America*, Claitor's Publish Division, Baton Rouge, p. 208.